






# Giant Cosmic-Ray Halos around M31 and the Milky Way

S. Recchia<sup>1,2,3,4</sup> , S. Gabici<sup>3</sup>, F. A. Aharonian<sup>5,6</sup> , and V. Niro<sup>3</sup> 

<sup>1</sup>Dipartimento di Fisica, Università di Torino, Via P. Giuria 1, 10125 Torino, Italy; [sarah.recchia@unito.it](mailto:sarah.recchia@unito.it)

<sup>2</sup>Istituto Nazionale di Fisica Nucleare, Sezione di Torino, Via P. Giuria 1, 10125 Torino, Italy

<sup>3</sup>Université de Paris, CNRS, Astroparticule et Cosmologie, F-75006 Paris, France

<sup>4</sup>IJCLab, CNRS/IN2P3, Université Paris-Saclay, F-91405 Orsay, France

<sup>5</sup>Dublin Institute for Advanced Studies, 31 Fitzwilliam Place, Dublin 2, Ireland

<sup>6</sup>Max-Planck-Institut für Kernphysik, Postfach 103980, D-69029 Heidelberg, Germany

Received 2021 January 13; revised 2021 April 16; accepted 2021 April 30; published 2021 June 24

## Abstract

Recently, a diffuse emission of 1–100 GeV  $\gamma$ -rays has been detected from the direction of M31, extending up to 200 kpc from its center. The interpretation of the extended  $\gamma$ -ray emission by the escape of cosmic rays produced in the galactic disk or in the galactic center is problematic. In this paper, we argue that a cosmic-ray origin (either leptonic or hadronic) of the  $\gamma$ -ray emission is possible in the framework of nonstandard cosmic-ray propagation scenarios or is caused by in situ particle acceleration in the galaxy's halo. Correspondingly, the halo is powered by the galaxy's nuclear activity or by the accretion of intergalactic gas. If the formation of cosmic-ray halos around galaxies is a common phenomenon, the interactions of cosmic-ray protons and nuclei with the circumgalactic gas surrounding the Milky Way could be responsible for the isotropic diffuse flux of neutrinos observed by IceCube.

*Unified Astronomy Thesaurus concepts:* Circumgalactic medium (1879); Andromeda Galaxy (39); Milky Way Galaxy (1054); Cosmic rays (329); Gamma-rays (637); Neutrino astronomy (1100)

## 1. Introduction

The Andromeda galaxy (M31), located at a distance of  $\sim 785$  kpc, is the closest spiral galaxy to the Milky Way (MW) and shares many similarities with the MW. Both galaxies are composed of a bulge, a disk, an extended gaseous halo, a central supermassive black hole (SMBH) and a dark matter halo that extends for 200–300 kpc (in radius) with a total mass of  $\sim 10^{12} M_{\odot}$  (see Karwin et al. 2019, and references therein).

Attempts to detect M31 in  $\gamma$ -rays date back to the seventies (Fichtel et al. 1975; Pollock et al. 1981; Sreekumar et al. 1994; Hartman et al. 1999), but high-energy photons have been detected only recently by Fermi-LAT (Abdo et al. 2010; Ögelman et al. 2011; Ackermann et al. 2017; Di Mauro et al. 2019). The integrated  $\gamma$ -ray luminosity above 100 MeV was found to be  $\sim 6.6 \times 10^{41} \text{ s}^{-1}$ , very close (within less than a factor of 2) to that of the MW (Abdo et al. 2010). While for the MW the emission correlates spatially with the gaseous disk, for M31 it appears to be concentrated within the inner  $\sim 5$  kpc region (Ackermann et al. 2017). The origin of the emission remains debated. Finally, some evidence for the existence of structures similar to the Fermi bubbles emanated from the central region of M31 has also been reported (Pshirkov et al. 2016).

Recently, an analysis of Fermi-LAT data revealed the presence of an extended  $\gamma$ -ray emission from a very large halo surrounding Andromeda (Karwin et al. 2019). The authors investigated a region of  $28^{\circ} \times 28^{\circ}$ , which includes a projected radius of  $\sim 200$  kpc from the center of M31. After performing accurate modeling of the MW foreground emission, they found an excess that extends up to about  $\sim 120$ – $200$  kpc around the center of M31. In order to better characterize such emission, they included in the analysis a spherically symmetric template centered on M31 and further divided into three regions: the inner galaxy (IG), a region of  $\sim 5.5$  kpc radius that contains the bright  $\gamma$ -ray emission from the IG (Ackermann et al. 2017), the spherical halo (SH), an intermediate ring that extends up to

$\sim 120$  kpc, and the outer halo (OH), a ring of  $\sim 120$ – $200$  kpc. The authors concluded that the excess emission indeed from comes M31 and estimated the total  $\gamma$ -ray flux and spectrum in the three regions.

Since the northern part of the considered regions, and especially that of the OH ring, partially overlaps with the disk of the MW, the authors also performed an additional analysis in which they reported separately the total flux and spectrum of the north and south parts of the intermediate (SH) and outer (OH) rings. While the north/south regions of the SH do not show relevant spectral differences, in the case of the OH the two spectra are quite different, with a bumpy profile in the northern part, showing a very likely contamination from the MW. Therefore, the authors conclude that, while the excess from the SH region is likely associated with the halo of M31, that from the OH region has a less clear origin, and could be partly or completely related to the MW, or even have another unspecified origin.

Based on the large extension of the emitting region, on the spectral shape and on the intensity of the various components, Karwin et al. (2019) suggest that while some fraction of the  $\gamma$ -ray emission could be due to cosmic-ray (CR) interactions in the halo of M31, it is unlikely that such CRs may dominate the production of  $\gamma$ -rays. Instead, they suggested that a dark matter interpretation could be a better explanation and described the details of such interpretation in a recent publication (Karwin et al. 2021).

As we argue in this paper, a CR origin for the extended emission is not only possible, but even quite natural. It would imply the existence of a giant CR halo of radius  $\sim 100$  kpc surrounding Andromeda and would require a nonstandard scenario for the transport of CRs into galactic halos. Remarkably, the existence of such large halos has been proposed for both the MW and M31 (Feldmann et al. 2013; Ahlers & Murase 2014; Taylor et al. 2014; Do et al. 2020). In particular, it was shown that the interaction of CRs in the diluted circumgalactic gas around the MW could explain the diffuse flux of neutrinos revealed by

IceCube (Taylor et al. 2014) and a subdominant fraction of the isotropic  $\gamma$ -ray background (Feldmann et al. 2013). The presence of a CR halo surrounding both the MW and M31 would support the similarities in the nonthermal properties of the two galaxies.

The outline of the paper is as follows: In Section 2, we summarize the relevant results of the analysis of Fermi-LAT from M31 reported by Karwin et al. (2019). In Section 3, we estimate the energy requirements for the hadronic or the leptonic origin of the  $\gamma$ -ray emission from the SH. In Section 4.1, we illustrate a scenario where CRs are produced during episodes of activity in the galactic center (GC) of M31 and then transported into the halo. In Section 4.2, we analyze a scenario where CRs are accelerated in situ at a gigantic shock located in the SH. In Section 5, we explore the multi-wavelength and multimessenger implications of a possible similarity between the halos surrounding M31 and the MW. A natural implication of this scenario is that IceCube neutrinos are originated in the extended halo of the MW. In Section 6, we discuss the implications of the existence of giant CR halos around more distant galaxies and compute the expected signals in multi-teraelectron/petaelectronvolt neutrinos and  $\gamma$ -rays from CR proton–proton interactions, along with the associated synchrotron emission from secondary electrons. We also briefly discuss the case of the galaxy NGC 1068 (Aartsen et al. 2020). In Section 7, we draw our conclusions.

## 2. Summary of the Relevant $\gamma$ -Ray Data

In this section we summarize the results of the analysis of Fermi-LAT from the M31 region performed in Karwin et al. (2019). We will not discuss here the bright  $\gamma$ -ray emission from the IG, whose origin has been debated in Ackermann et al. (2017), Di Mauro et al. (2019), and McDaniel et al. (2019), nor the tenuous diffuse emission from the OH, whose origin might be unrelated to M31 (Karwin et al. 2019), but we will rather focus on the  $\gamma$ -ray emission observed from the SH.

At the distance of M31, the radial extension of the SH with respect to the center of M31 is  $5.5 \text{ kpc} \lesssim r \lesssim 120 \text{ kpc}$ . It corresponds to a solid angle of  $3.42 \times 10^{-2} \text{ sr}$ . A spectral fit to the  $\gamma$ -ray emission observed from the SH was provided in Karwin et al. (2019), where a power-law plus exponential cutoff parameterization was adopted:

$$I_{\text{SH}} \approx 9.8 \times 10^{-11} E_{\text{GeV}}^{-1.9} e^{-E_{\text{GeV}}/11.6} \text{ MeV}^{-1} \text{ cm}^{-2} \text{ s}^{-1} \text{ sr}^{-1}, \quad (1)$$

where  $E_{\text{GeV}}$  is the photon energy in gigaelectronvolts (see Figure 1). In order to minimize the contamination from the MW, we consider only  $\gamma$ -ray data from the southern part of the SH. Also a pure power-law fit to the  $\gamma$ -ray emission from the (entire) SH was provided in Karwin et al. (2019). The results of the fit are shown in Figure 1 and were obtained using the Fermi Science Support Center Interstellar Emission Models (FSSC IEM).

The total  $\gamma$ -ray luminosity of the entire (northern plus southern part) SH equals

$$L_{\gamma} \approx 1.7 - 1.9 \times 10^{39} \text{ erg s}^{-1}, \quad (2)$$

where the lower value corresponds to the power-law plus cutoff fit to data and the upper value to the pure power-law case. In the following, we will consider both fits, and we will discuss

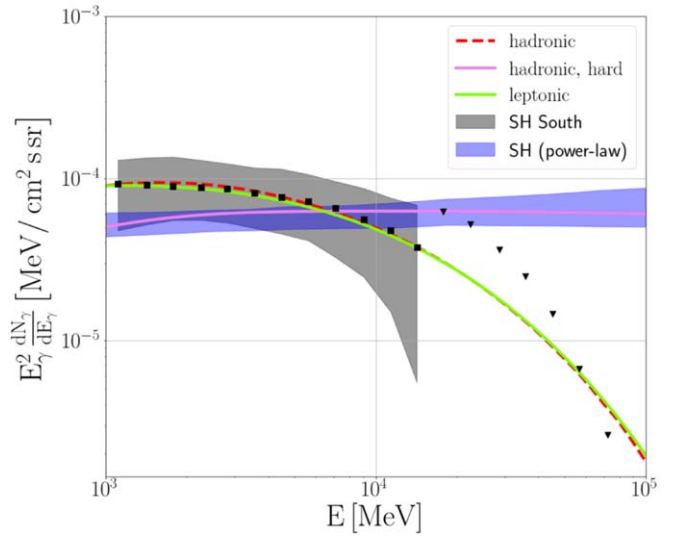


**Figure 1.** The black squares with the shaded region represent the the best fit to the  $\gamma$ -ray spectrum in the SH south, obtained by the analysis of Fermi-LAT in Karwin et al. (2019). The blue shaded region is a power-law fit to data (FSSC IEM analysis). The pink solid line represents the  $\gamma$ -ray flux in the case of the hard CR proton spectrum scenario considered in Section 5. The downward triangles are upper limits. The green solid (red dashed) line is a leptonic (hadronic) fit to data.

the profound implications of the presence or absence of a cutoff in the spectrum.

## 3. Hadronic and Leptonic Origin of the $\gamma$ -Ray Emission: Energetics

In this section we discuss a scenario where the  $\gamma$ -ray emission from the halo of M31 is produced by CR interactions, either hadronic or leptonic. In the former case,  $\gamma$ -rays are due to the decay on neutral pions produced in proton–proton interaction of CR protons with the diluted background gas in the halo, while in the latter they are produced via inverse Compton scattering (ICS) of CR electrons on cosmic microwave background (CMB) photons. Note that synchrotron losses on the background magnetic field are most likely negligible at distances exceeding a few tens of kiloparsecs from the disk, since the magnetic field strength there is expected to be well below  $\sim 3 \mu\text{G}$ , and therefore its energy density to be subdominant with respect to that of the CMB (Stanev 1997; Ferrière 2001; Jansson & Farrar 2012). In the following, under the assumption of stationarity, we compute the CR luminosity needed to explain the  $\gamma$ -ray emission from the SH.

### 3.1. Leptonic Scenario

In this scenario, the  $\gamma$ -ray emission from the halo is due to ICS of relativistic electrons off CMB photons. The average energy of such photons is  $\langle \epsilon_{\text{CMB}} \rangle \sim 6.3 \times 10^{-4} \text{ eV}$ . After the scattering, the photons are boosted to an energy (Blumenthal & Gould 1970) of

$$E_{\gamma} = \frac{4}{3} \gamma^2 \langle \epsilon_{\text{CMB}} \rangle \sim 3.2 E_{\text{TeV}}^2 \text{ GeV}, \quad (3)$$

where  $\gamma$  is the electron Lorentz factor and  $E_{\text{TeV}} = (E_e / 1 \text{ TeV})$  its energy in teraelectronvolts.

This implies that the diffuse  $\gamma$ -ray emission seen by Fermi-LAT at photon energies in the range of  $\sim 1\text{--}100 \text{ GeV}$  would be

produced by electrons of energy  $\sim 0.6\text{--}6\text{ TeV}$ . The cutoff energy in the  $\gamma$ -ray spectrum ( $E_\gamma = 11.6\text{ GeV}$ ) would correspond to electrons of energy  $E_{\text{max},e} \approx 1.9\text{ TeV}$ .

The IC energy loss rate for electrons in the CMB is given by Blumenthal & Gould (1970):

$$\frac{dE_e}{dt} = \frac{4}{3} \sigma_T c \gamma^2 \omega_{\text{CMB}} \sim 2.5 \times 10^{-2} E_{\text{TeV}}^2 \text{ eV s}^{-1}, \quad (4)$$

where  $\omega_{\text{CMB}} = 0.25\text{ eV cm}^{-3}$  is the energy density of CMB photons. The corresponding energy loss time is

$$\tau_{\text{CMB}} \equiv \frac{E_e}{dE_e/dt} \sim 1.3 \times 10^6 E_{\text{TeV}}^{-1} \text{ yr}. \quad (5)$$

This expression is valid in the Thomson limit, while at energies above  $\sim 10\text{ TeV}$  the Klein–Nishina effects becomes important (Blumenthal & Gould 1970). This quite short timescale makes it very unlikely that such electrons may originate in the galactic disk or from the GC. Even in the case of rectilinear (ballistic) motion, 3 TeV electrons would move at most  $\approx 100\text{ kpc}$  before cooling. But for any realistic diffusion such distance would be much smaller. Moreover, near the disk the energy loss time would be even shorter, due to the larger value of both the ambient magnetic field and the background photon field (starlight radiation plays a relevant role close to the disk). For these reasons, if the emission in the SH of M31 is of leptonic origin, the parent CR electron population is most likely accelerated in situ.

The minimal energy requirement for this leptonic scenario can be estimated by assuming that the age of the system and/or the residence time of electrons in the acceleration region is larger than the IC energy loss time. Under these circumstances, the  $\gamma$ -ray production happens in a calorimetric regime, namely, the observed  $\gamma$ -ray luminosity (Equation (2)) equals the electron luminosity

$$L_e = L_\gamma \approx 1.7 - 1.9 \times 10^{39} \text{ erg s}^{-1}. \quad (6)$$

Note that this estimate refers only to electrons in the energy band  $\approx 0.6\text{--}6\text{ TeV}$ . Such a luminosity is of the same order than the total estimated power of CR electrons accelerated in the disk of the MW (Strong et al. 2010).

A qualitative fit to the  $\gamma$ -ray flux is shown in Figure 1, which has been obtained assuming a CR electron spectrum of the form  $\propto E_{\text{GeV}}^{-2.0} e^{-E_{\text{GeV}}/500}$ . The ICS flux has been computed following Khangulyan et al. (2014).

### 3.2. Hadronic Scenario

In the hadronic scenario  $\gamma$ -rays of energy  $E_\gamma$  are produced in proton–proton interactions between CR protons of energy  $E_p \approx 10 E_\gamma$  and the ambient gas (Kelner et al. 2006). Moreover, the CR proton luminosity  $L_p$  needed to explain the observed  $\gamma$ -ray luminosity  $L_\gamma$  is given by Taylor et al. (2014):

$$L_p = \frac{3 L_\gamma}{f} \quad (7)$$

$$f = 1 - e^{-\tau_{\text{res}}/\tau_{\text{pp}}},$$

where  $\tau_{\text{res}}$  is the residence time of CRs in the halo and  $\tau_{\text{pp}}$  is the timescale for proton–proton interactions,

$$\tau_{\text{pp}} \sim 7.1 \times 10^{10} n_{\text{H},-3}^{-1} \text{ yr}, \quad (8)$$

where  $n_{\text{H},-3}$  is the halo hydrogen density in units of  $10^{-3}\text{ cm}^{-3}$ . The energy loss time  $\tau_{\text{pp}}$  has been computed for a cross section  $\sigma_{\text{pp}} \sim 3 \times 10^{-26}\text{ cm}^2$  and an inelasticity of the process  $\kappa \approx 0.5$ . Note that for  $n_{\text{H},-3} \lesssim 1$  the energy loss time largely exceeds the age of the universe. Typical values of  $n_{\text{H}}$  expected at  $\sim 100\text{ kpc}$  from the disk of the MW are  $\sim 10^{-4}\text{--}10^{-3}\text{ cm}^{-3}$  (Fang et al. 2012; Miller & Bregman 2013; Nuza et al. 2014; Miller & Bregman 2015), and therefore CR protons do not lose energy. Such gas densities are consistent with a number of observational measurements (Gupta et al. 2012), which were recently confirmed in Qu et al. (2021), where the authors found some evidence for the existence of a local hot bridge, i.e., a cylinder of radius  $\approx 120\text{ kpc}$  filled with hot gas connecting M31 to the MW.

Taking  $\tau_{\text{res}} = 10^9 \tau_{\text{res},9\text{ yr}}$  one can compute the CR proton luminosity needed to explain the  $\gamma$ -ray observations of the SH in M31:

$$L_p \approx 1.8 \times 10^{41} \tau_{\text{res},9}^{-1} n_{\text{H},-3}^{-1} \text{ erg s}^{-1}, \quad (9)$$

where a correction factor of  $\approx 2$  has been applied in order to account for the enhancement of the  $\gamma$ -ray emission due to the presence of heavy nuclei in both CR and ambient gas (Mori 1997; Caprioli et al. 2011; Kafexhiu et al. 2014). Note that for  $\tau_{\text{res},9} \gtrsim 1$  and  $n_{\text{H},-3} \sim 1$ , the luminosity of CR protons needed to account for the  $\gamma$ -ray emission from the SH is of the same order of that invoked to explain the population of CR protons observed in the disk of the MW (Strong et al. 2010).

A qualitative fit to the  $\gamma$ -ray flux is shown in Figure 1, which has been obtained assuming a CR proton spectrum  $\propto E_{\text{GeV}}^{-2.0} e^{-E_{\text{GeV}}/110}$  or  $\propto E_{\text{GeV}}^{-2.0}$  for the power-law plus cutoff and pure power-law scenario, respectively. The emission from proton–proton interactions has been computed following Kelner et al. (2006) and Kamae et al. (2008).

If the CR proton luminosity  $L_p$  is stationary over a time  $\tau_{\text{res}}$ , then the total energy in form of CR protons in the SH would be  $L_p \times \tau_{\text{res}}$ , which would result in an average CR energy density of the order of

$$\omega_{\text{CR},p} = \frac{L_p \tau_{\text{res}}}{V_{\text{SH}}} \sim 0.017 n_{\text{H},-3}^{-1} \text{ eV cm}^{-3}, \quad (10)$$

where  $V_{\text{SH}}$  is the volume of the SH region. This is much smaller (about a factor of 50) than the typical energy density of CRs in the disk of the MW. However, it should be considered as a lower limit of the CR density, since the CR proton population could be distributed in a fraction of the SH volume, depending on the scenario invoked for its origin (as shown in what follows).

## 4. Origin of the Radiating Particles

As seen in the previous section, the luminosity in form of energetic particles needed to explain the  $\gamma$ -ray halo of M31 is comparable to the CR luminosity of the MW. This is true for both the hadronic and the leptonic scenario (see Equations (6) and (9)). As M31 and the MW are two galaxies of the same type and of comparable masses, it is reasonable to assume that their CR energy outputs should also be of the same order.

According to the standard model for CR origin (see, e.g., Gabici et al. 2019), such energetic particles are accelerated at sources (maybe SNRs) located in the disk of the MW. The injection of CR particles in the interstellar medium is balanced



by their escape from the Galaxy, which is due to a combination of spatial diffusion (random scattering in the turbulent galactic magnetic field) and advection (due to the presence of a galactic wind). Therefore, one might envisage a scenario where CRs (protons and/or electrons) would be accelerated at SNRs in the disk of M31 or injected from the GC, and then transported into the extended halo where they would interact with ambient gas and/or radiation fields to produce the observed  $\gamma$ -ray emission.

However, such a scenario would not work. As seen in the previous section, the problem with electrons is their very short radiative timescale, which would prevent them from being transported to large distances from the disk. For protons, the problem is related to their advective/diffusive transport from the disk/GC to the halo. Predictions from standard models involving a turbulent ambient magnetic field and a galactic wind invariably predict a decreasing intensity of CR protons for larger distances from the disk/GC (see Kalashev & Troitsky 2016 and the Appendix for more details). Thus, in order to fit the  $\gamma$ -ray flux observed from the SH, a very large intensity of CR protons must be present in the disk of M31, which should therefore be observed as a bright  $\gamma$ -ray source. As the gaseous disk is not bright in  $\gamma$ -rays, we conclude that a CR origin of the  $\gamma$ -ray emission from the halo of M31 requires going beyond the standard scenario for the production and transport of CRs in normal galaxies.

In this section, we explore two scenarios for the production of the energetic particles responsible for the  $\gamma$ -ray emission from the SH. We consider first a model where CR protons are produced in the GC of M31 and are then transported into the halo by means of buoyant bubbles. In such scenario, the problem of a substantial decrease of the CR density with the distance from the GC can be overcome.

Then we consider a scenario where particles (either protons or electrons) are produced in situ, as a result of the acceleration at a gigantic shock located in the SH. Such a shock might be either an accretion shock or the termination shock generated by a galactic outflow.

#### 4.1. Activity of the GC

The discovery of the Fermi bubbles in the MW is a spectacular signature of past nuclear activity in our galaxy (Su et al. 2010). They are two symmetric  $\gamma$ -ray emitting bubbles extending up to a distance of  $\gtrsim 10$  kpc above and below the galactic disk (Ackermann et al. 2014). Very recently, the X-ray counterparts of Fermi bubbles have been observed (Predehl et al. 2020).

Due to the similarity with the MW we will assume here that episodes of nuclear activity also happens in M31 (we remind that the existence in M31 of structures similar to the Fermi bubbles has been proposed based on Fermi-LAT observations (Pshirkov et al. 2016)). The origin of Fermi bubbles is still debated. They could be inflated as the result of either intense star formation in the GC (e.g., Crocker & Aharonian 2011) or accretion/ejection processes at the central SMBH (e.g., Guo & Mathews 2012). The two scenarios involve mechanisms operating over different timescales (from a few to a few tens of megayears) and injecting energy at different rates (from  $\lesssim 10^{41}$  to  $\approx 10^{43}$  erg s $^{-1}$ ), with overall energetics in the range spanning from  $W_B \approx 10^{55}$  up to a few times  $10^{57}$  erg (Guo & Mathews 2012; Miller & Bregman 2016; Barkov & Bosch-Ramon 2014; Yang et al. 2012).

Here, we investigate a scenario where CR protons are produced in recurring episodes of nuclear activity in M31,

similar to that responsible for the creation of the Fermi bubbles in the MW, and are then transported into the extended halo inside buoyant bubbles. If  $\nu_B = 10^{-2} \nu_{B,-2}$  Myr $^{-1}$  is the frequency of the episodes of nuclear activity in M31, the effective rate at which CR protons may be injected into the halo is

$$L_p = \eta E_B \nu_B \sim 3.2 \times 10^{41} \eta E_{B,57} \nu_{B,-2} \text{ erg s}^{-1}, \quad (11)$$

where  $E_{B,57} = E_B 10^{-57}$  erg and  $\eta$  is an efficiency that takes into account the fact that only a fraction of the total energy involved in the process is converted into CRs. The efficiency also accounts for possible adiabatic energy losses that particles may experience during the transport to the halo. After comparing this expression with the energy requirement in Equation (9) one gets

$$\eta \approx 0.56 \tau_{\text{res},9}^{-1} n_{\text{H},-3}^{-1} E_{B,57}^{-1} \nu_{B,-2}^{-1}, \quad (12)$$

which is tight but not at all unfeasible. For example, a moderate efficiency at the percent level could be achieved by considering a confinement time of CRs close to the age of the system ( $\tau_{\text{res}} 9 \sim 10$ ) and a typical energetic for a single episode of nuclear activity characterized by values of  $E_{B,57}$  of the order of a few (comparable to the estimate made in Yang et al. 2012 for the energetic Fermi bubbles).

The transport of CR protons from the GC to the halo must proceed in such a way to prevent particles to return to the disk and avoid in this way an overproduction of  $\gamma$ -rays there, due to proton-proton interactions in the interstellar gas. This requirement might be accommodated, for example, by assuming that CR-inflated-buoyant bubbles carry energetic particles to large distances from the disk, before being disrupted by plasma instabilities (Gull & Northover 1973). Such buoyant bubbles, often present in the central regions of clusters of galaxies (Churazov et al. 2001; Jones & De Young 2005), have also been observed in galaxies (Finoguenov et al. 2008).

Bubbles are typically found to rise at a buoyant velocity of the order of a fraction of the sound of speed (which is  $\sim 100$  km s $^{-1}$  for the typical temperature of the hot diffuse circumgalactic gas (Zhang et al. 2018)), while their typical lifetime could be as low as  $\approx 10^8$  yrs (Churazov et al. 2001; Jones & De Young 2005; Zhang et al. 2018), or significantly longer, even beyond  $\sim 10^9$  yr if the stabilizing action of a magnetic field is invoked (see Zhang et al. 2018 and references therein). For a bubble lifetime of  $\sim 10^9$  yr and a sound of speed of  $100$  km s $^{-1}$ , every bubble would bring CRs up to a distance of  $\lesssim 100$  kpc from the disk before releasing them in the halo (Jones & De Young 2005; Zhang et al. 2018).

Once released in the galactic halo, CRs will spread diffusively to fill a region of  $\approx 100$  kpc radius, as indicated by the extension of the  $\gamma$ -ray emission in the SH. The time needed to fill such region depends on the CR diffusion coefficient  $D$ , which under most circumstances is an increasing function of particle energy.

For particle energies for which the diffusion time  $\tau_{\text{res}} \sim R_{\text{SH}}^2 / (6D)$  over a region of size  $R_{\text{SH}} \sim 100$  kpc is shorter than the typical time between episodes of nuclear activity  $1/\nu_B$ , the contributions of several bubbles in the SH overlap and the CR population in that region and at those particle energies is stationary. This happens for protons of energy smaller than  $E_c$ , when the diffusion coefficient is smaller than the critical value  $D(E) < D(E_c) = 5 \times 10^{30} R_{100}^2 \nu_{B,-2} \text{ cm}^2 \text{ s}^{-1}$ . On the other

hand, protons of energy larger than  $E_c$  will populate the halo intermittently. For this reason, a cutoff in the proton spectrum will occasionally appear, and could explain the power-law plus cutoff fit to  $\gamma$ -ray data (black points in Figure 1), provided that  $E_c \approx 100$  GeV. Note that the corresponding diffusion coefficient for  $E = E_c$  would be somewhat larger than the value usually quoted for galactic CR propagation at this energy (Strong et al. 2007). However, at the large distances from the disk considered here, an increase of the diffusion coefficient compared to the near-disk region may indeed be expected (Ptuskin et al. 1997; Strong et al. 2007; Recchia et al. 2016).

A radically different scenario can be envisaged, if the diffusion coefficient is rather flat in energy, and/or if all CR protons injected during the entire lifetime of M31 are confined in the SH. In this case, no cutoff is expected in the spectrum, which could extend well beyond the gigaelectronvolt domain. This would be consistent with the pure power-law fit to data (purple shaded region in Figure 1). We will explore the implications of this scenario in Sections 5 and 6.

It is important to emphasize that the CR transport in the SH by mean of buoyant bubbles is substantially different from the case in which particles diffuse/advection directly from the GC region of M31. As shown in the Appendix, the last scenario would imply either a very small emissivity in the SH or a very bright emission in the IG, which, however, is not observed. However, in the buoyant bubble scenario, particles start to diffuse only when the bubble is disrupted and they are already in the SH. This situation is somewhat similar to the case of continuous injection (which is a good approximation when the contributions of different bubbles overlap) and diffusion from a source (as described in the Appendix), but with the source being in the SH rather than in the GC. This would produce a quasi-stationary CR population in the SH without affecting the IG/disk region (see also the discussion below). In the IG, a possibly intermittent Fermi bubble-like structure may be observed.

We conclude this section by noting that the presence of a large scale galactic wind or outflow might prevent particles injected in the SH from coming back to the disk. Such outflow could be the responsible for the presence of target material at  $\sim 100$  kpc (see, e.g., Miller & Bregman 2015; Recchia 2020). Let us assume that CRs are released by a buoyant bubble at a distance  $R_*$  from the disk. It would take a time of  $t_* \approx R_*^2 6 D^{-1}$  to spread over a region of size  $R_*$ . For a galactic wind velocity  $u_{\text{out}} = 10^3 u_{\text{out},3}$  km s $^{-1}$  (Recchia 2020) the condition of non-return to the disk is then  $t_* \gtrsim R_*/u_{\text{out}}$ . This translates into another constraint on the particle diffusion coefficient:  $D \lesssim 5 \times 10^{30} R_{*,2} u_{\text{out},3} \text{ cm}^2 \text{ s}^{-1}$ , where  $R_* = 10^2 R_{*,2}$  kpc.

#### 4.2. In Situ Acceleration of Electrons and Protons

As seen in Section 3.1, a leptonic origin of the  $\gamma$ -ray emission from the SH requires an acceleration of electrons in situ. Therefore, here we explore a scenario where CR electrons are accelerated at a giant strong shock located in the SH of M31.

The maximum energy  $E_{\text{max},e}$  of accelerated electrons at a spherical shock of radius  $R_s$  can be estimated by equating the acceleration timescale  $\tau_{\text{acc}} \sim a D(E_e)/u_s^2$  (Drury 1983) to the energy loss time  $\tau_{\text{loss}} = E_e/(dE_e/dt)$ . Here,  $u_s = 10^3 u_{s,3}$  km s $^{-1}$  is the velocity at which matter flows into the shock,  $dE_e/dt$  is the ICS energy loss rate (see Equation (4)), and  $a \approx 10$  is a numerical factor that depends on how much the shock

compresses the gas and the magnetic field (see e.g., Gaggero et al. 2018). Assuming Bohm diffusion,  $D = R_L(E_e)c/3$  with  $R_L$  the particle Larmor radius, the resulting maximum energy is

$$E_{\text{max},e} \approx 34 a_1^{-1} u_{s,3} B_{-6}^{1/2} \text{ TeV}, \quad (13)$$

where  $a = 10 a_1$ .

The strength of the magnetic field in the halo of galaxies is a poorly constrained quantity. However, it is believed that particle acceleration at shocks is accompanied by an amplification of the field (Bell 2004). From observations of galactic SNRs, it has been inferred that a fraction  $\xi_B \approx 3.5\%$  of the shock ram pressure is converted into magnetic field energy (Völk et al. 2005), i.e., where the subscript  $d$  indicates that the magnetic field has been measured downstream of the shock, while  $\rho_0$  is the gas mass density of the intergalactic medium upstream of the shock. By substituting this expression in Equation (13) one finally gets

$$E_{\text{max},e} \approx 24 u_{s,3}^3 n_{0,-4}^{1/4} \left( \frac{\xi_B}{0.035} \right)^{1/4} \text{ TeV}, \quad (14)$$

where  $n_0 = 10^{-4} n_{0,-4} \text{ cm}^{-3}$  is the number density of the intergalactic gas.

Since the observed  $\gamma$ -ray spectrum extends up to at least a photon energy  $E_\gamma \approx 10$  GeV, the electron spectrum should extend at least up to an energy  $E_{\text{max},e} \approx 2$  TeV. This conditions is satisfied if

$$u_{s,3} \gtrsim 0.43 n_{0,-4}^{-1/12} \left( \frac{\xi_B}{0.035} \right)^{-1/12}. \quad (15)$$

This velocity is remarkably close to the freefall velocity at the edge of the SH:

$$v_{\text{ff}} \sim 0.29 \times 10^3 M_{12}^{1/2} R_{\text{SH},2}^{-1/2} \text{ km s}^{-1}, \quad (16)$$

where  $M = 10^{12} M_{12}$ ,  $M_\odot$  is the total mass of M31. We note, also, that the radius of the SH,  $R_{\text{SH}} = 100 R_{\text{SH},2}$  kpc, is of the same order of the virial radius of the system. We may speculate, then, that particles are accelerated at a spherical accretion shock, that would process free-falling intergalactic matter. Energy would flow across the shock at a rate of

$$L_s \approx (4\pi R_{\text{SH}}^2) \frac{\rho_0 v_{\text{ff}}^3}{2} \sim 3.4 \times 10^{42} R_{\text{SH}}^{1/2} n_{0,-4} M_{12}^{3/2} \text{ erg s}^{-1}, \quad (17)$$

which could very easily satisfy the energy requirement expressed by Equation (6). While we note that particle acceleration at accretion shocks is very often invoked around clusters of galaxies (Blasi et al. 2007), we should keep in mind that the very existence of accretion shocks around galaxies is debated (Birnbom & Dekel 2003; Ji et al. 2021).

It is interesting to note that, even in the absence of an accretion shock, the presence of an incoming flow may help in confining CRs due to an inward advection term. Using Equation (16), the inflowing material may confine CRs in the SH within a region of

$$R_{\text{vff}} \approx 180 \frac{D_{30}}{v_{\text{ff},2}} \text{ kpc}, \quad (18)$$

where  $D_{30}$  is the diffusion coefficient in units of  $10^{30} \text{ cm}^2 \text{ s}^{-1}$  (which roughly corresponds to the typical CR galactic diffusion

coefficient at petaelectronvolt energies) and  $v_{\text{ff},2}$  is the freefall velocity in units of  $10^2 \text{ km s}^{-1}$ .

Another possibility is that the shock is formed as the result of the nuclear activity in the GC. Following Cheng et al. (2011) and Miller & Bregman (2016) we may obtain a very rough estimate of the radius  $R_s$  and expansion velocity  $u_s$  of the shock by means of an analogy with wind blown bubbles. If  $L_{\text{GC}} = 10^{43} L_{\text{GC},43} \text{ erg s}^{-1}$  is the time-averaged rate of energy injection in the bubble due to galactic nuclear activity, we have (Weaver et al. 1977):

$$R_s \approx \left( \frac{L_{\text{GC}}}{\rho_0} \right)^{1/5} t^{3/5}, \quad u_s = \frac{3 R_s}{5 t}. \quad (19)$$

After setting  $R_s \sim R_{\text{SH}}$  and  $t \sim \tau_{\text{GC}}$ , where  $\tau_{\text{GC}} = 10^9 \tau_{\text{GC},9} \text{ yr}$  overall duration of the nuclear activity (which may also consist of a number of recurrent episodes), we get

$$u_s \approx 0.2 \times 10^3 L_{\text{GC},43}^{1/5} n_{0,-4}^{-1/5} \tau_{\text{GC},9}^{-2/5} \text{ km s}^{-1}, \quad (20)$$

where we normalized the energy injection rate to a very small fraction of the Eddington luminosity of the central SMBH of mass  $M_{\text{BH}}$  (Ghisellini 2013):

$$L_{\text{Edd}} \sim 1.3 \times 10^{46} \left( \frac{M_{\text{BH}}}{10^8 M_{\odot}} \right) \text{ erg s}^{-1}. \quad (21)$$

In order to provide the CR electron luminosity needed to explain observations (Equation (6)) the acceleration efficiency of electrons at the accretion shock must be of the order of  $\eta_e \sim 5 \times 10^{-4} R_{\text{SH}}^{-1/2} n_{0,-4}^{-1} M_{12}^{-3/2}$ . With efficiency we mean here the fraction of the energy flowing across the shock, which is converted into the CR electrons responsible for the  $\gamma$ -ray emission. In the scenario where the shock is generated as a consequence of the galactic nuclear activity, a fraction  $\eta_e \sim 2 \times 10^{-4} L_{\text{GC},43}^{-1}$  of the power injected into the system has to be converted into CR electrons.

An important aspect of a leptonic origin of the emission is the morphology. In fact, given the short lifetime of the electrons in the energy range relevant for the  $\gamma$ -ray data (see Equation (5)), they would fill just a thin shell of  $R(1 \text{ TeV}) \approx 4 \sqrt{D_{30}}$  kpc, where  $D_{30}$  is the diffusion coefficient in units of  $10^{30} \text{ cm}^2 \text{ s}^{-1}$ . This would be seen in  $\gamma$ -rays as a thin bright rim. The detection of such morphology would indicate that at least part of the emission is leptonic.

Besides electrons, also CR protons will be accelerated at the shock, most likely with a much larger efficiency, as inferred from the study of galactic CRs (Strong et al. 2010). The maximum energy of accelerated protons  $E_{\text{max},p}$  can be obtained, in this case, by equating the acceleration time  $\tau_{\text{acc}}$  to the age of the shock  $\tau_s = 10^9 \tau_{s,9} \text{ yr}$  (which is of the order of  $\tau_{\text{age}}$  for the accretion shock or  $\tau_{\text{GC}}$  for the shock formed due to the nuclear activity), as proton-proton interactions are an extremely inefficient energy loss mechanism (see Equation (8)).

In fact, another condition should be satisfied in order to have acceleration up to the highest energies: particles must remain confined in the accelerator. This is equivalent to impose that the diffusion length of protons of energy  $E_{\text{max},p}$  should be smaller than the size of the accelerator ( $\sim R_{\text{SH}}$ ). The two conditions result in very similar values for  $E_{\text{max},p}$ , so we consider here the

former, which gives

$$E_{\text{max},p} \approx 4.6 \times 10^2 u_{s,3}^3 \tau_{s,9} n_{0,-4}^{1/2} \left( \frac{\xi_B}{0.035} \right)^{1/2} \text{ PeV}, \quad (22)$$

showing that the acceleration of CR protons can proceed up to very high energies, well beyond the  $\sim 10$ – $100$  TeV needed to explain the  $\gamma$ -ray observations. The  $\gamma$ -ray emission from the halo can be explained if the acceleration efficiency of protons at the accretion shock is of the order of  $\eta_p \sim 0.01 R_{\text{SH}}^{-1/2} n_{0,-4}^{-2} M_{12}^{3/2}$ , where we assumed that CR protons remain trapped downstream of the shock for the entire lifetime of the system ( $\tau_{\text{res}}, 9 \sim 10$ ). In the galactic nuclear activity scenario, the efficiency would be  $\eta_p \sim 5 \times 10^{-3} n_{0,-4}^{-1} L_{\text{GC},43}^{-1}$ .

The shock in SH could originate also at the termination of the galactic wind powered by the sources located in the disk. However, in this case the required energetics is less affordable compared to the above cases. Indeed, in order to provide the required proton luminosity given by Equation (9), for the acceleration efficiency at the level of 10%, the shock's luminosity power should exceed  $10^{42} \text{ erg s}^{-1}$ , which is comparable to the collective SNR power in the MW.

We conclude this section by noting that so far we have made the implicit assumption that the shock in the SH is strong and non-radiative, i.e., characterized by a shock compression factor  $r = 4$ . Given the low density and large temperature  $T > 10^6 \text{ K}$  in the halo, the shock would become radiative in a time  $\tau_{\text{cool}} \approx \epsilon / \Lambda \approx 1 n_{0,-4}^{-1} (T / 3 \times 10^6 \text{ K})^{3/2} \text{ Gyr}$ , where  $\epsilon$  is the thermal energy density of the gas and the Kahn approximation has been adopted for the cooling coefficient  $\Lambda \approx 10^{-19} T^{-1/2} \text{ erg cm}^3 \text{ s}^{-1}$  (Cox 2005). Note that here  $T$  is assumed to be the temperature downstream of the shock. This implies that an hypothetical shock in the SH might become radiative. Even though it is often assumed in the literature that radiative shocks are not efficient particle accelerators, recent studies seem to suggest, instead, that acceleration efficiency at the percent level, similar to that required in our scenario, is indeed possible (Steinberg & Metzger 2018).

## 5. A Giant CR Halo around the MW and the Origin of IceCube Neutrinos

We now turn our attention to the MW. The existence of a giant ( $\sim 100$ – $200$  kpc) CR halo surrounding our galaxy was proposed in Taylor et al. (2014) as an explanation of the diffuse flux of multi-teraelectronvolt neutrinos detected by IceCube (IceCube Collaboration 2013).

The differential isotropic flux of astrophysical neutrinos (all flavors, neutrinos plus antineutrinos) measured at Earth can be fitted with a power law (Abbasi et al. 2020):

$$\Phi_{\nu}^{\text{IC}}(E_{\nu}) \sim 6.37 \times 10^{-18} \left( \frac{E_{\nu}}{100 \text{ TeV}} \right)^{-2.87} \text{ GeV}^{-1} \text{ cm}^{-2} \text{ s}^{-1} \text{ sr}^{-1}. \quad (23)$$

The data reported in Abbasi et al. (2020) refer to particle energies above  $\approx 100$  TeV, and therefore the integrated isotropic flux is  $F_{\nu}(>100 \text{ TeV}) \sim 1.2 \times 10^{-10} \text{ erg cm}^{-2} \text{ s}^{-1} \text{ sr}^{-1}$ . Assuming that the observed neutrinos are produced in the halo of the MW, at a typical distance of  $R_{\text{H}} = 10^2 R_{\text{H},2} \text{ kpc}$ , then the differential neutrino emissivity from the entire MW is

$$Q_{\nu}^{\text{MW}}(E_{\nu}) = (4\pi)^2 \Phi_{\nu}^{\text{IC}}(E_{\nu}) R_{\text{H}}^2 \quad (24)$$



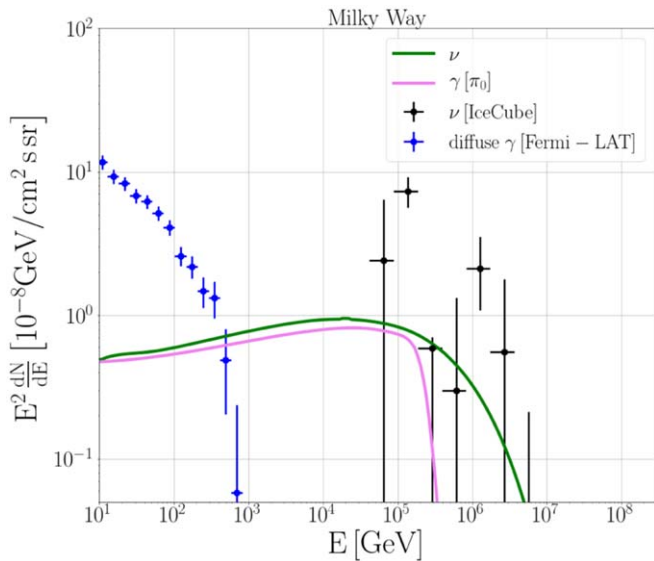


**Figure 2.** Isotropic diffuse neutrino and  $\gamma$ -ray emission observed by IceCube (Abbasi et al. 2020, black) and Fermi-LAT (Ackermann et al. 2015, blue data points). Solid lines are predictions for the neutrino (green) and  $\gamma$ -ray (pink) resulting from the interactions of CR protons with ambient gas in a  $\sim 100$  kpc halo surrounding the MW.

and the related luminosity can be estimated as

$$L_{\nu}^{\text{MW}}(>100 \text{ TeV}) \approx 1.8 \times 10^{39} R_{\text{H},2}^2 \text{ erg s}^{-1}. \quad (25)$$

If the neutrinos are the result of the decay of charged pions generated in proton–proton interactions in the circumgalactic gas, then an isotropic diffuse  $\gamma$ -ray emission above  $\sim 100$  TeV is also expected, with a luminosity comparable to that of neutrinos.

The isotropic diffuse fluxes of  $\gamma$ -rays and neutrinos measured by Fermi-LAT (Ackermann et al. 2015) and IceCube (Abbasi et al. 2020), respectively, are shown in Figure 2, together with the predictions from the  $\gamma$ -ray and neutrino emission from CR proton–proton interactions in the MW halo. Predictions have been computed assuming a proton spectrum  $\propto E_p^{-2} \exp(-E_p/20 \text{ PeV}^{-1})$  normalized in such a way to contain a total energy equal to  $W_p^{-2} 4.6 \times 10^{57} R_{\text{H},2}^2 n_{\text{H},-3}^{-1} \text{ erg}$ .

The abrupt cutoff in the  $\gamma$ -ray spectrum reflects the fact that very high-energy photons are absorbed due to pair production in the CMB (Veronetti & Lipari 2016). Absorption has been computed assuming photons traveled 100 kpc.

It is interesting to note that such scenario would imply a recovery of the isotropic diffuse  $\gamma$ -ray emission above a photon energy of  $E_{\gamma} \approx 1 \text{ TeV}$ , at a level of  $\sim 10^{-8} \text{ GeV cm}^2 \text{ s}^{-1} \text{ sr}^{-1}$ , and extending up to  $E_{\gamma} \lesssim 1 \text{ PeV}$ . Available upper limits from observations performed at photon energies above  $\sim 100 \text{ TeV}$  sit at about the same level (Apel et al. 2017).

It seems natural, at this point, to compare the two hadronic scenarios proposed above to explain the  $\gamma$ -ray and neutrino production in the halo of the MW and M31, respectively. The observational constraints for the gas density in the halos of the two galaxies give very similar values (see, e.g., Gupta et al. 2012; Qu et al. 2021). On the other hand, the CR proton content in the halo would scale linearly with the central SMBH mass in a scenario where the acceleration of particles is connected to galactic nuclear activity (see Equation (21)) or with the total mass of the galaxy to the power 3/2 in an accretion scenario (see Equation (17)). The ratio between the

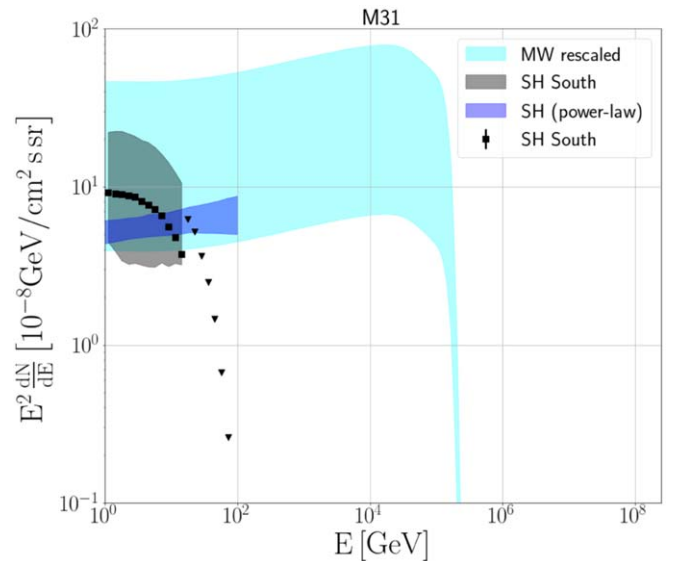


**Figure 3.** Expected  $\gamma$ -ray emission from M31 (cyan shaded region) obtained rescaling the predictions shown in Figure 2 for the halo of the MW. The black data points and the gray shaded region show Fermi-LAT observations of M31 (Karwin et al. 2019).

mass of M31 and of the MW is  $\sim 2$  (Peñarrubia et al. 2014), while the ratio between the SMBH masses is  $\sim 33$  (Bender et al. 2005). Therefore, assuming that the two galaxies can confine CRs for comparable times, one would expect the  $\gamma$ -ray and neutrino luminosities of M31 to exceed those of the MW by a factor of  $\approx 2.8$ –33. Such rescaled fluxes are shown in Figure 3, together with the spectrum of M31 observed by Fermi-LAT for a power-law plus exponential cutoff modeling of data (black points and gray shaded region) and for a power-law model (blue line and shaded region) (Karwin et al. 2019). The power-law model derives from a less sophisticated analysis of Fermi-LAT, but is claimed to be consistent with the more sophisticated approach. The good match between our prediction and Fermi-LAT suggests a possible common origin of the giga-electronvolt  $\gamma$ -ray emission from the halo of M31 and the neutrino emission from the halo of the MW. A firm assessment of the presence or not of a cutoff/steepening in the giga-electronvolt  $\gamma$ -ray spectrum of M31 will be a crucial test for this scenario.

The large field of view and the superior sensitivity of the Large High Altitude Air Shower Observatory (LHAASO) detectors (Bai et al. 2019) should be able to detect the multi-teraelectronvolt  $\gamma$ -ray emission from M31, which implies that the scenario we propose will be tested in the near future.

Finally, another consequence of the similarity between M31 and MW is that, as pointed out already in Taylor et al. (2014), multi-teraelectronvolt CRs have to be confined in the galactic halos for long times, of the order of gigayears, to maintain the global energy budget at the levels discussed in Section 3.

## 6. Multiwavelength and Multimessenger Implications

In the scenario described above, the  $\gamma$ -ray emission observed from the halo of M31 is the result of CR proton–proton interactions with the circumgalactic gas. If, as suggested in the previous section, the spectrum of protons extends up to petaelectronvolt energies, then the halo will also emit multi-teraelectronvolt/petaelectronvolt  $\gamma$ -rays and neutrinos. However,

it is straightforward to show that, according to the scenario illustrated in Figure 3, M31 should provide only a minor contribution (about  $\approx 5\%$ ) to the total isotropic flux observed by IceCube (the number of neutrinos in the IceCube high-energy starting event sample considered here is 60 (Abbasi et al. 2020)). Moreover, neutrinos from M31 would come from a very extended region of apparent size (diameter)  $\approx 15^\circ R_{H,2}$ .

Assuming that all galaxies similar to the MW are surrounded by a giant CR halo, we can estimate their contribution to the isotropic diffuse neutrino flux. If such a flux is in fact dominated by the emission coming from the MW halo, the contribution from other galaxies must be subdominant. This leads to the condition

$$E_\nu^2 \Phi_\nu^{\text{IC}}(E_\nu) \gtrsim \frac{c\tau_{\text{max}}}{4\pi} E_\nu^2 Q_\nu^{\text{MW}}(E_\nu) n_{\text{gal}}, \quad (26)$$

where we ignored the redshift evolution of sources, and assumed that only sources located within a distance  $c\tau_{\text{max}}$  contribute to the diffuse flux. Here,  $n_{\text{gal}} = 10^{-2} n_{\text{gal},-2} \text{ Mpc}^{-3}$  is the density of galaxies in the local universe. The maximum distance  $c\tau_{\text{max}}$  should be interpreted as follows: as it takes a long time, comparable to the age of the universe, to fill galactic halos with CRs, only old and massive galaxies in the nearby universe are expected to be bright neutrino emitters. The constraint expressed by Equation (26) is satisfied when  $(c\tau_{\text{max}}) \lesssim 3 \text{ Gpc}$ , where we made use of Equation (24) and we set  $n_{\text{gal},-2} \sim 0.3$ , which is an appropriate value for galaxies of mass comparable to that of the MW (Blanton & Moustakas 2009). We note that a very similar argument proposing that our galaxy could be a typical emitter of high-energy neutrinos and therefore could potentially provide a sizable fraction of the diffuse flux measured by IceCube was put forward in Gallo Rosso et al. (2018).

The discovery potential of a point source for IceCube currently corresponds to a flux level of  $\gtrsim 10^{-12} \text{ TeV cm}^{-2} \text{ s}^{-1}$ , if the source spectrum is  $\propto E_\nu^{-2}$  (Aartsen et al. 2020). The halo of a galaxy like M31 would appear as point-like (smaller than a degree) if located at distances larger than  $\gtrsim 10 \text{ Mpc}$ . At that distance, the neutrino flux of a M31-like galaxy would be of the order of  $\approx 2 \times 10^{-14} \text{ TeV cm}^{-2} \text{ s}^{-1}$ , a couple of orders of magnitude below the detection limit. This implies that only galaxies characterized by an enhanced nuclear or starburst activity could be seen as neutrino sources. This is particularly relevant in connection with the recent claim by the IceCube Collaboration of a  $\lesssim 3\sigma$  excess of very high-energy neutrinos from the galaxy NGC 1068, located at a distance of 14.4 Mpc (Aartsen et al. 2020). This galaxy exhibits both active galactic nuclei and starburst activity, and therefore it seems to be an ideal neutrino emitter. However, the non-detection of very high-energy  $\gamma$ -rays from this object (Aartsen et al. 2020) challenges an interpretation of the neutrino excess based on proton–proton interactions from the extended disk/halo region. A possible combined explanation of  $\gamma$ -ray and neutrino observations of NGC 1068 was recently proposed in Inoue et al. (2020). Deeper observations in both neutrinos and  $\gamma$ -rays will help in clarifying this issue.

The secondary electrons from interactions of accelerated protons with the circumgalactic gas result in nonthermal X-radiation. The latter is contributed by ultrahigh energy (petaelectronvolt) electrons through synchrotron radiation and relatively low energy (gigaelectronvolt) electrons through ICS

on the 2.7 K cosmic microwave background radiation (CMBR). The characteristic energies of X-rays produced through these channels are

$$E_X \approx 2 B_{-7} E_{e,\text{PeV}}^2 \text{ keV} \quad (27)$$

and

$$E_X \approx 4 E_{e,\text{GeV}}^2 \text{ keV}, \quad (28)$$

respectively. Here,  $B_{-7}$  is the magnetic field strength in the halo in units of  $10^{-7} \text{ G}$  and  $E_{e,\text{PeV}} = E_e \text{ PeV}^{-1}$  and  $E_{e,\text{GeV}} = E_e \text{ GeV}^{-1}$ .

The cooling time of gigaelectronvolt electrons is very large,

$$\tau_{\text{CMB}}(E_e) \approx 10^9 E_{e,\text{GeV}}^{-1} \text{ yr}. \quad (29)$$

Therefore, the contribution of ICS of gigaelectronvolt electrons to the X-ray emission of extended galactic sources such as SNRs and pulsar wind nebulae, is negligible. However, in the scenarios proposed here, the parent CR protons are assumed to be confined in galactic halos for  $\tau_{\text{res}} \gtrsim 10^9 \text{ yr}$ . This implies a very high (close to 100%) efficiency of conversion of the kinetic energy of secondary electrons to IC X-rays, taking into account that for the typical magnetic field in the halo,  $B \lesssim 10^{-7} \text{ G}$ , the electrons are cooled predominantly through ICS on the 2.7 K CMBR.

For the timescales exceeding the IC cooling time of electrons given by Equation (29), the equilibrium electron spectrum is given by

$$N_e(E_e) = \frac{\int_{E_e}^{E_{\text{max}}} q_e(E) dE}{|b(E_e)|}, \quad (30)$$

where  $q_e(E_e)$  is the injection spectrum of secondary electrons and  $b_e(E_e) \propto E_e^2$  is the ICS energy loss rate in the Thompson regime. For the  $E_p^{-2}$  type parent proton spectrum,  $q_e \propto E_e^{-2}$ , and consequently the ICS cooling of electrons results in the equilibrium spectrum  $N_e \propto E_e^{-3}$ . Correspondingly, the X-ray IC spectrum is  $\propto E^{-2}$ . For the  $E^{-2}$  type spectrum of protons extending to petaelectronvolt energies, more than 10% is contained in  $\leq 100 \text{ GeV}$  protons responsible for secondary electrons, and then in IC X-rays. Taking into account that the production rate of electrons from the decays of secondary charged mesons is comparable to the production rate of neutrinos, the emissivity of X-rays is estimated at the level of 10% of the overall neutrino luminosity, namely,

$$\Phi(1 - 100 \text{ keV}) \approx 10^{-3} \text{ keV cm}^{-2} \text{ s sr}. \quad (31)$$

This flux is significantly below the extragalactic diffuse X-ray background (Gilli et al. 2007). For the halo of the MW, it corresponds to the global X-ray luminosity of the MW halo of the order of  $L_{X,1-100 \text{ keV}}^{\text{MW}} \approx 2 \times 10^{37} R_{H,2}^2 \text{ erg s}^{-1}$ . The halo of a galaxy similar to the MW located at a distance  $d$  would be characterized by a X-ray flux and an angular extension equal to  $\approx 6 \times 10^{-14} R_{H,2}^2 (d/3 \text{ Mpc})^{-2} \text{ erg cm}^2 \text{ s}^{-1}$  and  $\vartheta_H \sim 2^\circ R_{H,2} (d/3 \text{ Mpc})^{-1}$ , respectively. The very large extension of the source could make a detection of such a signal problematic.

High-energy electrons, in the energy range of  $\approx 0.7\text{--}7 \text{ PeV}$  also contribute to the 1–100 keV X-ray flux. However, given



the small value of the magnetic field in the halo, the contribution is  $\lesssim 10^{-2}$  times smaller than that reported in Equation (31). The suppression factor is given by the ratio  $\tau_{\text{ICS}}/\tau_{\text{syn}}$  at the considered high energies. Taking into account the Klein–Nishina regime in ICS, such ratio at  $E_e \sim 1$  PeV is  $\approx 0.04 B_{-7}^2$ .

## 7. Conclusions

The existence of a very extended ( $\approx 100$  kpc) gaseous halo around the MW has been revealed by a number of X-ray observations (see, e.g., Gupta et al. 2012). If found to be a common feature of galaxies, gaseous halos might solve the problem of missing baryons in the universe. In Taylor et al. 2014, it was proposed that, besides solving this problem, such gaseous halos could also shine in very high-energy  $\gamma$ -rays and neutrinos, due to the interactions between CR protons and ambient gas. It was shown that, under certain assumptions on the CR luminosity of the MW, the neutrino emission from the halo could explain the diffuse flux of neutrinos measured by IceCube.

In this paper we investigated the observational consequences that the presence of a similar halo would have for M31, the closest massive galaxy to the MW. We were motivated by the recent discovery in Fermi-LAT of a giant  $\gamma$ -ray halo of size  $\sim 100$ – $200$  kpc surrounding the galaxy.

Our main conclusion is that, provided CRs can be confined for long times (comparable to the age of the system) in the halos, both the isotropic diffuse neutrino emission observed by IceCube, and the extended  $\gamma$ -ray emission measured by Fermi-LAT around M31 could be explained in terms of CR interactions with the circumgalactic gas.

We showed that such large halos may be explained through CR protons produced in the GC of M31 and then transported into the halo by means of buoyant bubbles, or in a scenario where CRs, either electrons or protons, are accelerated in situ at a large shock in the SH region. In the former case, the morphology of the emission from M31 is expected to be similar to that of Fermi bubbles, but much more extended, while in the latter case, the emission is expected to be roughly spherically symmetric.

The time-averaged luminosity of CRs to be injected into the halo is of the order of  $\gtrsim 10^{40}$ – $10^{41}$  erg  $s^{-1}$ , comparable to the estimated luminosity of CR sources in the galactic disk. The scenario we propose is testable, as it predicts a multi-teraelectronvolt  $\gamma$ -ray emission from the halo of M31 that is within the reach of instruments such as LHAASO.

If all galaxies are surrounded by gaseous halos, then they might all emit both  $\gamma$ -rays and neutrinos. However, given the performances of current instruments, we estimated that the detection of galaxies located at distances significantly larger than M31 would be possible only in the presence of an enhanced nuclear or starburst activity, that could boost the acceleration of CRs. A very recent claim from the IceCube Collaboration on a  $\lesssim 3\sigma$  excess from the direction of NGC 1068, a Seyfert-type galaxy exhibiting starburst activity and located at a distance of 14.4 Mpc, might fit with this prediction. On the other hand, the lack of  $\gamma$ -ray emission from that object poses problems to any interpretation of data based on CR interactions with the gas in an extended disk/halo system.

We conclude by recalling that an alternative and viable scenario to interpret the observations of M31 could involve

leptonic interactions (namely, ICS) operating in its halo. Of course, in this case no neutrinos would be expected from M31.

The authors would like to thank M. Brueggen for helpful discussions, and the anonymous referee for insightful comments. S.R. and S.G. acknowledge support from the region Île-de-France under the DIM-ACAV program, from the Agence Nationale de la Recherche (grant ANR- 17-CE31-0014), and from the Observatory of Paris (Action Fédératrice CTA). This project has received funding from the European Union’s Horizon 2020 research and innovation program under the Marie Skłodowska-Curie grant agreement No. 843418 (nuHEDGE).

## Appendix Standard Models of CR Propagation

The extended  $\gamma$ -ray emission of M31 is very hard to be accounted for in the standard scenario in which CRs are generated by galactic accelerators, e.g., by SNRs or the GC, located in the galactic disk and in typical scenarios of CR propagation from the disk. This is obvious for CR electrons, which would not be able to travel  $\sim 100$  kpc even considering only losses due to ICS on the CMB. As for CR protons, we show that, in any common transport scenario the CR density inevitably decreases significantly with the distance from the disk. Moreover, the gas density is also expected to decrease appreciably, and observations of the MW halo confirm such trend (Miller & Bregman 2013, 2015). This is at odds with the detected  $\sim 100$  kpc extended emission. Moreover, as we show below, given the observed  $\gamma$ -ray emissivity in the SH, any such propagation scenario would imply a very large  $\gamma$ -ray emissivity in the disk of M31, which however is not observed.

In standard models of CR propagation, CRs are expected to diffuse away from the disk while being scattered on plasma waves. Such waves could be injected in the disk by astrophysical sources (Evoli et al. 2018) or could be produced by the CR streaming instability (Kulsrud & Pearce 1969; Skilling 1975; Blasi 2019). However, in both cases, the magnetic turbulence is expected to decrease away from the disk, resulting in a CR diffusion coefficient that tends to increase with the distance from the disk. In such scenario, CRs are expected to free stream above few kiloparsecs from the disk (Blasi 2013; Amato 2014). Evidently all this would lead to a (fast) decrease of the CR density toward the outer halo. This conclusion also does not change in more complex models, involving, together with diffusion, the possible presence of a galactic wind that advects CRs (and which could be responsible for the presence of target material at  $\sim 100$ – $200$  kpc from the disk of Andromeda).

In what follows, we analyze in detail some typical propagation setups, showing that they would inevitably lead either to a very faint emissivity in the SH or to a very large emissivity in the disk or IG of M31.

The best-fit intensities, in units of  $\text{MeV}^{-1} \text{cm}^{-2} \text{s}^{-1} \text{sr}^{-1}$ , for the IG ( $r \lesssim 5.5$  kpc, solid angle of  $1.44 \times 10^{-4}$  sr) and the SH ( $5.5 \text{ kpc} \lesssim r \lesssim 120$  kpc, solid angle of  $3.42 \times 10^{-2}$  sr) are given by

$$\begin{aligned} I_{\text{IG}} &\approx 6.4 \times 10^{-9} E_{\text{GeV}}^{-2.8} e^{-E_{\text{GeV}}/100} \\ I_{\text{SH}} &\approx 9.8 \times 10^{-11} E_{\text{GeV}}^{-1.9} e^{-E_{\text{GeV}}/11.6}. \end{aligned} \quad (\text{A1})$$

The ratio between the average  $\gamma$ -ray emissivity of the two regions is

$$\frac{\langle \epsilon_{\text{SH}} \rangle}{\langle \epsilon_{\text{IG}} \rangle} \sim 10^{-3}. \quad (\text{A2})$$

### A.1. Stationary Diffusion from a Continuous Source

Let us imagine that CR protons are continuously injected at a point source (e.g., the GC of M31) and are subject to a diffusion coefficient  $D(E, r)$ . Neglecting any other effect, the transport equation for the CR distribution function reads as

$$\frac{\partial f(E, r, t)}{\partial t} = \vec{\nabla} \cdot (D(E, r) \vec{\nabla} f(E, r, t)) + Q(E) \delta(\vec{r}). \quad (\text{A3})$$

In the steady-state regime and in spherical coordinates the solution satisfies, in terms of spatial profile (see, e.g., Kalashev & Troitsky 2016),

$$r^2 D(r) \frac{\partial f(r)}{\partial r} = \text{const}, \quad (\text{A4})$$

namely, assuming that the CR diffusion coefficient increases as  $D(r) \propto r^\alpha$

$$f(r) \propto r^{-1-\alpha}. \quad (\text{A5})$$

Note that in the case of free-streaming  $f(r) \propto r^{-2}$ . In the most optimistic scenario of a spatially constant diffusion coefficient (as explained above,  $D(r)$  is indeed expected to increase with the distance from the disk) we would expect  $f(\text{IG})/f(\text{R}_{\text{SH}}) \sim 100 R_{\text{SH},2}$ . If, in addition, we take into account the different gas density in the IG and SH regions, we would get

$$\frac{\langle \epsilon_{\text{SH}} \rangle}{\langle \epsilon_{\text{IG}} \rangle} \propto \frac{f_{\text{SH}} n_{\text{SH}}}{f_{\text{IG}} n_{\text{IG}}} \approx 10^{-5} \frac{n_{\text{SH},-3}}{n_{\text{IG},0}}, \quad (\text{A6})$$

where we used  $n_{\text{IG}} \sim 1 \text{ cm}^{-3}$  and  $n_{\text{SH}} \sim 10^{-3} \text{ cm}^{-3}$ . Any increase of  $D$  with  $r$  would inevitably lead to a faster decrease of the CR density and to a decrease of such ratio. However, the observed ratio is given by Equation (A2). This tells us that, if we fix the CR density, and consequently the emissivity, in the IG, and we assume that the emission is dominated by proton–proton interactions both in the IG and in the SH, the emission in the SH should be much fainter than observed. Or, if we fix the emissivity in the SH, the IG should be much brighter than observed.

### A.2. Stationary Diffusion from the Galactic Disk

The analysis presented for a continuous point source can be extended to the case of continuous injection from sources located in the disk of M31. In typical models of galactic CR propagation (see, e.g., Gabici et al. 2019; Recchia 2020 for a review), CRs are assumed to diffuse away from the disk along a magnetic flux, in a diffusive halo whose size is typically set to few kiloparsecs. Outside the diffusive halo, CRs are assumed to free stream to infinity (the diffusion coefficient becomes extremely large), and a free escape boundary is often imposed at the outer edge of the diffusive halo. Evidently, in such scenario the CR density in the SH would be vanishingly small.

A less extreme situation could be envisaged by taking into account a possible increase of  $D(z)$  with the distance  $z$  from the disk, and the possible geometry of the flux tube, typically expected to be nearly cylindrical up to distances from the disk smaller or comparable to the disk radius ( $\sim 10$ – $15$  kpc for the MW and M31), and with a spherical opening at larger distances. Thus, introducing the flux tube area  $A(z)$ , and assuming that the CR sources are solely in the disk (see e.g. Breitschwerdt et al. 1991; Everett et al. 2008; Recchia et al. 2016, 2017), one gets for the CR density

$$A(z) D(z) \frac{\partial f}{\partial z} = \text{const}, \quad (\text{A7})$$

similar to Equation (A4). Considering that  $A(z) \propto z^2$  above few kpc, the conclusions on the CR density in the SH are similar to the case of diffusion from a continuous point source.

### A.3. Galactic Winds

Also galactic winds have been invoked in models of CR propagation. Following the approach by Breitschwerdt et al. (1991); Everett et al. (2008); Recchia et al. (2016, 2017), in a stationary wind/breeze model, characterized by the flux tube area  $A(z)$ , with  $z$  the distance from the disk, the gas  $n(z)$  density and velocity  $u(z)$ , and the CR pressure  $P_c(z)$  are related by conservation laws

$$\begin{aligned} n u A &= \text{const} \\ P_c(u A) \gamma_c &= \text{const}, \end{aligned} \quad (\text{A8})$$

where  $\gamma_c$  is the adiabatic index of the CR gas ( $\gamma_c = 4/3$  for relativistic particles). At large enough  $z$ , the flux tube is expected to open up spherically see discussion above and the gas density is observed to decrease with  $z$  (Miller & Bregman 2013, 2015). Moreover, at large  $z$  the wind velocity becomes constant, while it decreases with  $z$  in the case of breeze. We get

$$\begin{aligned} A(z) &\propto z^2 \\ u(z) &\propto z^{-\beta} \\ n(z) &\propto z^{\beta-2} \\ P_{c(z)} &\propto z^{(\beta-2)\gamma_c}. \end{aligned} \quad (\text{A9})$$

Here,  $\beta < 2$  (otherwise  $n$  would increase with  $z$ ) and  $\beta = 0$  for a wind. Thus, in both cases the CR pressure would decrease with  $z$ . In addition, Recchia et al. (2016) showed that in a wind the CR spectrum tends to become progressively harder with  $z$ , thus enhancing the decrease of the CR density at energies below  $\sim 1000$  GeV.

Recently, an interesting self-confinement scenario was put forward by Blasi & Amato (2019) and Blasi (2019) in the case of the MW. The idea is that the CR current of CRs produced in the disk and trying to free stream to infinity in a progressively smaller background magnetic field, leads to the excitation of a nonresonant plasma instability, the Bell instability. As far as the CR propagation perpendicular to the disk can be considered as one-dimensional, the instability induces a strong amplification of the background magnetic field and a suppression of the CR diffusion coefficient. This happens for distances from the disk smaller than roughly the disk radius  $R_d$  ( $\sim 10$  kpc for both M31 and the MW). The instability is excited on scales much smaller than the Larmor radius of CRs and saturates when the

scale becomes comparable to the Larmor radius. In addition, the resulting large CR pressure gradient leads to a displacement of the background medium at a speed that is roughly at the level of the Alfvén speed computed in the amplified magnetic field. The resulting confinement time in a region of  $\simeq 10$  kpc can be as large as  $\sim 10^8$ – $10^9$  yr.

The instability is excited only if the background magnetic field is smaller than the saturation value

$$B_{\text{sat}} \approx 2.2 \times 10^{-8} L_{41}^{1/2} r_{10}^{-1} \text{ G}, \quad (\text{A10})$$

where  $L_{41}$  is the CR luminosity in units of  $10^{41}$  erg s $^{-1}$  and  $r_{10}$  is the size of the CR source region (e.g., the disk) in units of 10 kpc. CR diffusion is expected to proceed at the Bohm limit in the saturated magnetic field and CR will experience an advection velocity, respectively, given by

$$D(E) \approx 1.5 \times 10^{24} E_{\text{GeV}} L_{41}^{-1/2} r_{10} \text{ cm}^2 \text{ s}^{-1} \\ \tilde{v}_A \approx 5 L_{41}^{1/2} r_{10}^{-1} n_{-4}^{-1/2} \text{ km s}^{-1}. \quad (\text{A11})$$

However, at distances larger than  $\sim R_d$ , the one-dimension propagation assumption is no more valid, the CR density tends to decrease spherically and the self-confinement becomes quickly inefficient (Blasi & Amato 2019; Blasi 2019). Thus, even in a scenario of strong CR confinement, the CR density is expected to rapidly drop with the distance from the disk.

### ORCID iDs

S. Recchia  <https://orcid.org/0000-0002-1858-2622>  
 F. A. Aharonian  <https://orcid.org/0000-0003-1157-3915>  
 V. Niro  <https://orcid.org/0000-0003-4409-6852>

### References

- Aartsen, M. G., Ackermann, M., Adams, J., et al. 2020, *PhRvL*, **124**, 051103  
 Abbasi, R., Ackermann, M., Adams, J., et al. 2020, arXiv:2011.03545  
 Abdo, A. A., Ackermann, M., Ajello, M., et al. 2010, *A&A*, **523**, L2  
 Ackermann, M., Ajello, M., Albert, A., et al. 2015, *ApJ*, **799**, 86  
 Ackermann, M., Ajello, M., Albert, A., et al. 2017, *ApJ*, **836**, 208  
 Ackermann, M., Albert, A., Atwood, W. B., et al. 2014, *ApJ*, **793**, 64  
 Ahlers, M., & Murase, K. 2014, *PhRvD*, **90**, 023010  
 Amato, E. 2014, *IJMPD*, **23**, 1430013  
 Apel, W. D., Arteaga-Velázquez, J. C., Bekk, K., et al. 2017, *ApJ*, **848**, 1  
 Bai, X., Bi, B. Y., Bi, X. J., et al. 2019, arXiv:1905.02773  
 Barkov, M. V., & Bosch-Ramon, V. 2014, *A&A*, **565**, A65  
 Bell, A. R. 2004, *MNRAS*, **353**, 550  
 Bender, R., Kormendy, J., Bower, G., et al. 2005, *ApJ*, **631**, 280  
 Birnboim, Y., & Dekel, A. 2003, *MNRAS*, **345**, 349  
 Blanton, M. R., & Moustakas, J. 2009, *ARA&A*, **47**, 159  
 Blasi, P. 2013, *A&ARv*, **21**, 70  
 Blasi, P. 2019, *Galax*, **7**, 64  
 Blasi, P., & Amato, E. 2019, *PhRvL*, **122**, 051101  
 Blasi, P., Gabici, S., & Brunetti, G. 2007, *IJMPA*, **22**, 681  
 Blumenthal, G. R., & Gould, R. J. 1970, *RvMP*, **42**, 237  
 Breitschwerdt, D., McKenzie, J. F., & Voelk, H. J. 1991, *A&A*, **245**, 79  
 Caprioli, D., Blasi, P., & Amato, E. 2011, *Aph*, **34**, 447  
 Cheng, K. S., Chernyshov, D. O., Dogiel, V. A., Ko, C. M., & Ip, W. H. 2011, *ApJL*, **731**, L17  
 Churazov, E., Brügggen, M., Kaiser, C. R., Böhringer, H., & Forman, W. 2001, *ApJ*, **554**, 261  
 Cox, D. P. 2005, *ARA&A*, **43**, 337  
 Crocker, R. M., & Aharonian, F. 2011, *PhRvL*, **106**, 101102  
 Di Mauro, M., Hou, X., Eckner, C., Zaharijas, G., & Charles, E. 2019, *PhRvD*, **99**, 123027  
 Do, A., Duong, M., McDaniel, A., et al. 2020, arXiv:2012.14507  
 Drury, L. O. 1983, *RPPH*, **46**, 973  
 Everett, J. E., Zweibel, E. G., Benjamin, R. A., et al. 2008, *ApJ*, **674**, 258  
 Evoli, C., Blasi, P., Morlino, G., & Aloisio, R. 2018, *PhRvL*, **121**, 021102  
 Fang, T., Bullock, J., & Boylan-Kolchin, M. 2012, *ApJ*, **762**, 20  
 Feldmann, R., Hooper, D., & Gnedin, N. Y. 2013, *ApJ*, **763**, 21  
 Ferrière, K. M. 2001, *RvMP*, **73**, 1031  
 Fichtel, C. E., Hartman, R. C., Kniffen, D. A., et al. 1975, *ApJ*, **198**, 163  
 Finoguenov, A., Ruszkowski, M., Jones, C., et al. 2008, *ApJ*, **686**, 911  
 Gabici, S., Evoli, C., Gaggero, D., et al. 2019, *IJMPD*, **28**, 1930022  
 Gaggero, D., Zandanel, F., Cristofari, P., & Gabici, S. 2018, *MNRAS*, **475**, 5237  
 Gallo Rosso, A., Mascaretti, C., Palladino, A., & Vissani, F. 2018, *EPJP*, **133**, 267  
 Ghisellini, G. 2013, Radiative Processes in High Energy Astrophysics, Lect. Notes Phys., 873 (Berlin: Springer)  
 Gilli, R., Comastri, A., & Hasinger, G. 2007, *A&A*, **463**, 79  
 Gull, S. F., & Northover, K. J. E. 1973, *Natur*, **244**, 80  
 Guo, F., & Mathews, W. G. 2012, *ApJ*, **756**, 181  
 Gupta, A., Mathur, S., Krongold, Y., Nicastro, F., & Galeazzi, M. 2012, *ApJL*, **756**, L8  
 Hartman, R. C., Bertsch, D. L., Bloom, S. D., et al. 1999, *ApJS*, **123**, 79  
 IceCube Collaboration 2013, *Sci*, **342**, 1242856  
 Inoue, Y., Khangulyan, D., & Doi, A. 2020, *ApJL*, **891**, L33  
 Jansson, R., & Farrar, G. R. 2012, *ApJ*, **757**, 14  
 Ji, S., Kereš, D., Chan, T. K., et al. 2021, *MNRAS*, **505**, 259  
 Jones, T. W., & De Young, D. S. 2005, *ApJ*, **624**, 586  
 Kafexhiu, E., Aharonian, F., Taylor, A. M., & Vila, G. S. 2014, *PhRvD*, **90**, 123014  
 Kalashev, O., & Troitsky, S. 2016, *PhRvD*, **94**, 063013  
 Kamae, T., Karlsson, N., Mizuno, T., Abe, T., & Koi, a. 2008, *ApJ*, **647**, 692  
 Karwin, C., Murgia, S., Moskalenko, I., et al. 2021, *Phys. Rev. D*, **103**, 023027  
 Karwin, C. M., Murgia, S., Campbell, S., & Moskalenko, I. V. 2019, *ApJ*, **880**, 95  
 Kelner, S. R., Aharonian, F. A., & Bugayov, V. V. 2006, *PhRvD*, **74**, 034018  
 Khangulyan, D., Aharonian, F. A., & Kelner, S. R. 2014, *ApJ*, **783**, 100  
 Kulsrud, R., & Pearce, W. P. 1969, *ApJ*, **156**, 445  
 McDaniel, A., Jeltama, T., & Profumo, S. 2019, *PhRvD*, **100**, 023014  
 Miller, M. J., & Bregman, J. N. 2013, *ApJ*, **770**, 118  
 Miller, M. J., & Bregman, J. N. 2015, *ApJ*, **800**, 14  
 Miller, M. J., & Bregman, J. N. 2016, *ApJ*, **829**, 9  
 Mori, M. 1997, *ApJ*, **478**, 225  
 Nuza, S. E., Parisi, F., Scannapieco, C., et al. 2014, *MNRAS*, **441**, 2593  
 Ögelman, H., Asaker, N., Anilin, S., et al. 2011, in AIP Conf. Ser., 1379, ed. E. Göğüş, T. Belloni, & Ü. Ertan (New York: AIP), 82  
 Peñarrubia, J., Ma, Y.-Z., Walker, M. G., & McConnachie, A. 2014, *MNRAS*, **443**, 2204  
 Pollock, A. M. T., Bignami, G. F., Hermsen, W., et al. 1981, *A&A*, **94**, 116  
 Predehl, P., Sunyaev, R. A., Becker, W., et al. 2020, *Natur*, **588**, 227  
 Pshirkov, M. S., Vasiliev, V. V., & Postnov, K. A. 2016, *MNRAS*, **459**, L76  
 Ptuskin, V. S., Voelk, H. J., Zirakashvili, V. N., & Breitschwerdt, D. 1997, *A&A*, **321**, 434  
 Qu, Z., Huang, R., Bregman, J. N., & Li, J.-T. 2021, *ApJ*, **907**, 14  
 Recchia, S. 2020, *IJMPD*, **29**, 2030006  
 Recchia, S., Blasi, P., & Morlino, G. 2016, *MNRAS*, **462**, 4227  
 Recchia, S., Blasi, P., & Morlino, G. 2017, *MNRAS*, **470**, 865  
 Skilling, J. 1975, *MNRAS*, **173**, 245  
 Sreekumar, P., Bertsch, D. L., Dingus, B. L., et al. 1994, *ApJ*, **426**, 105  
 Steaver, T. 1997, *ApJ*, **479**, 290  
 Steinberg, E., & Metzger, B. D. 2018, *MNRAS*, **479**, 687  
 Strong, A. W., Moskalenko, I. V., & Ptuskin, V. S. 2007, *ARNPS*, **57**, 285  
 Strong, A. W., Porter, T. A., Digel, S. W., et al. 2010, *ApJL*, **722**, L58  
 Su, M., Slatyer, T. R., & Finkbeiner, D. P. 2010, *ApJ*, **724**, 1044  
 Taylor, A. M., Gabici, S., & Aharonian, F. 2014, *PhRvD*, **89**, 103003  
 Vernetto, S., & Lipari, P. 2016, *PhRvD*, **94**, 063009  
 Völk, H. J., Berezhko, E. G., & Ksenofontov, L. T. 2005, *A&A*, **433**, 229  
 Weaver, R., McCray, R., Castor, J., Shapiro, P., & Moore, R. 1977, *ApJ*, **218**, 377  
 Yang, H. Y. K., Ruszkowski, M., Ricker, P. M., Zweibel, E., & Lee, D. 2012, *ApJ*, **761**, 185  
 Zhang, C., Churazov, E., & Schekochihin, A. A. 2018, *MNRAS*, **478**, 4785